EPITAXIAL GROWTH OF GALLIUM ARSENIDE WITH AMMONIUM HALIDES AS TRANSPORTING AGENTS

by

He Bong Kim

Richard L. Longini

Prepared under Contract No. NAS 8-5269 by
Carnegie Institute of Technology
Pittsburgh, Pennsylvania
for
National Aeronautics and Space Administration

EPITAXIAL GROWTH OF GALLIUM ARSENIDE WITH AMMONIUM HALIDES AS TRANSPORTING AGENTS

32109

I. INTRODUCTION

The epitaxial growth of gallium arsenide on gallium arsenide are made utilizing the "close-spaced" source-seed ensemble in a closed system. Combinations of the low index orientations of {100}, {110}, and {111} as well as the polycrystalline samples, are used to determine the relative rates of the nucleation and growth on the low index orientations. Stacking faults, dislocations, and twin boundaries are observed and their configurations are studied. Early stages of the growth on the low index crystallographic orientations are observed and the configurations of the growth are compared with the etch pits. The rates of growth on the low index planes determined by the "close-spaced" epitaxial growth, can probably be explained by the "atomistic" model of the growth of facets proposed by Faust and John[1].

Ammonium halides such as NH_4Cl, NH_4I, and NH_4Br are shown to be useful transporting agents of gallium arsenide. The equilibrium behavior of the ammonium halide (i.e. NH_4Cl) - gallium arsenide system is studied to provide a firm foundation for a basic understanding of the system. The composition of the gas phase in equilibrium with solid GaAs is calculated for various temperatures, pressures, and component ratios. The principle species under equilibrium conditions are H_2, N_2, $GaCl_3$, HCl, As_4, NH_4Cl, GaCl, NH_3, and $AsCl_3$.

II. THERMODYNAMIC EQUILIBRIUM BEHAVIOR OF THE SYSTEM

An examination of thermodynamic data was made to aid in identifying the reacting species in the system and to determine the principle chemical equilibria involved for temperatures ranging from 700 to 1200°K. In order to determine partial, component, and total pressures, the conditions were assumed to be near thermodynamic equilibrium. Calculations were made relative to the following species: $H_2(g)$, $Cl_2(g)$, HCl(g), $N_2(g)$, $NH_3(g)$, $NH_4Cl(g)$, GaCl(g),

$GaCl_3(g)$, $As_4(g)$, $AsCl_3(g)$, and GaAs(s). Data on enthalpies and entropies for the various species are from Kubaschewski and Evans[2] Kelley[3], McBride[4], Stull and Sinke[5], Stull[6], Bichowsky[7], Latimer[8], and Gabor[9]. Other species were assumed negligible in this temperature range.

The system at equilibrium may be represented by the basic chemical reactions of Table I. Other reactions can be derived from them. Applying the law of mass action, the equilibrium equations with the equilibrium constant, K, are also given.

The equilibrium constants are determined from the data of Tables III and IV through the equation $\ln K = \frac{1}{R}\left(\Delta S_T - \frac{\Delta H_T}{T}\right)$, where ΔH_T and ΔS_T denote the enthalpies and entropies of formation respectively. In Table V the free energies of formation are listed for the reactions. $[X_i]$ denotes the partial pressure of species X_i. The conservation equations of components $\boxed{Cl_2}$, $\boxed{H_2}$, and $\boxed{N_2}$, where the boxes represent total quantities, are given in Table II. It can be seen that the boxed quantities must be constant in the reaction given in equations (1) through (6).

Equation 18 of Table II is obtained from the relationship of the stoichiometry between gallium and arsenic in GaAs. As gallium appears or disappears so must arsenic. In this case the $\langle\ \rangle$ represents excess arsenic. This is also the conservation equation for gallium.

The equations (7) through (16) with the various initial conditions and the calculated equilibrium constants, were solved to obtain partial pressures of the species with respect to temperatures ranging from 700° to 1200°K (with a Burrough computer). The initial conditions considered here are given in grams introduced into the closed system (20 cm^3 in volume). The total pressure is computed to be in the range of from one to five atmospheres, and in this range it is reasonable to approximate using Gibbs free energy and Helmholtz free energy interchangeably. Hence the calculation presented here may be used for the cases where the constraints are either the temperature and volume or the temperature and pressure. The initial conditions are adjusted appropriately for each case. Figures 1, 2, and 3 show the partial pressure of

each species with respect to temperature with the initial conditions of $[NH_4Cl]$ = 2 mg, <As> = 0; $[NH_4Cl]$ = 5 mg, <As> = 0; and of $[NH_4Cl]$ = 15 mg, <As> = 0. The $Cl_2(g)$ species is not shown in the figure as it is negligible compared to the other species for the temperature ranges considered. Figure 4 shows the partial pressures as a function of the initial conditions, <As>, and shows component ratio, $\frac{(As)}{Cl}$, with $[NH_4Cl]$ of 5 mg at 963°K. In Figure 5 the partial pressures of species are shown as a function of the component ratio, $\frac{(Ga)}{Cl}$, and of the initial condition, $[NH_4Cl]$, with zero excess arsenic and a temperature of 963°K. In Figure 6, the component ratio, $\frac{(Ga)}{Cl}$, is shown as a function of temperature at various $[NH_4Cl]$ and no excess arsenic, while in Figure 7, it is shown for $[NH_4Cl]$ of 5 mg and various <As>. The application of the preceeding equilibrium data on the ammonium chloride - gallium arsenide system may be demonstrated by the use of Lever's [11,12] model developed for steady-state diffusion-limited transport of solids in the presence of several chemical equilibria. Calculations using the values at the equilibrium cannot, as a general rule, predict exactly what happens in the vapor growth experiment as kinetic factors are often of great importance. The equilibrium information enables one to obtain some idea of the deviations to be expected and of the kinetic driving forces.

III. EXPERIMENTAL PROCEDURE

A closed tube system is chosen for its simplicity of use in conjunction with the ammonium halides (NH_4Cl, NH_4I, and NH_4Br).

GaAs seed and source wafers are polished using a mechanical polishing as well as chemical polishing techniques. For {100}, {110}, and {111}B crystal orientations, the chemically polished surface was prepared by etching in H_2SO_4 (98%) : H_2O_2 (30%) : H_2O :: 8 : 1 : 1. The wafer was fastened to a flat quartz plate, and rotated on another plate within a rotating beaker. For {111}A polishing an etch of 4-6 percent sodium hypochloride at 75°C was employed. It was mechanically polished on a rotating pellon cloth using first a premixed solution of Linde A : H_2O : H_2O_2 :: 10 : 4 : 1 and then a solution of Linde B : H_2O : H_2O_2 :: 10 : 5 : 1 by volume. The amonium halides used in the system

are refined in a multiple chamber vacuum distillation tube to remove the residues and the volatile impurities.

The prepared samples were loaded into a clean quartz system as shown in Figure 8 together with the ammonium halide and other components designed to provide various growth conditions. The ampule was evacuated to about 10^{-7} torr, sealed off and placed in the furnace which had the temperature profile, measured without the ampule, as shown in Figure 9. The separation distance between the seed and source wafers ranged from 0.25 to 1.0 mm and the spacer was a quartz ring. The two thermocouples shown in Figure 8 measure the average growth temperature, T_{av}, during the growth run.

IV. RESULTS

The rates of the growth are found to be dependent on several parameters involved in the system, such as the separation distance of the seed and source wafers, d, the temperature difference, $\Delta T = T_1 - T_2$ where T_1 is the temperature at the source and T_2 is the temperature at the seed, the average growth temperature, $T_{av} = \frac{(T_1 + T_2)}{2}$, and the initial conditions, which include the amount of impurities, the amonium halides, the nonstoichiometric excess arsenic initially introduced, the crystallographic orientations of the seed and source, and the surface conditions. The results presented hereafter refer only to the "close-spaced" epitaxial growth with the ammonium chloride as the transporting agent, unless otherwise designated. T_1 and T_2 were not measured under operating conditions at the source and seed but were temperatures taken at the side.

Epitaxial overgrowth of gallium arsenide on gallium arsenide, using an ammonium chloride carrier, are shown in Figure 10. The photomicrograph of the overgrowth on the polycrystalline substrate, as shown in Figure 10(A), resembles the substrate in its crystallographic orientations. Figure 10(B) is the photomicrograph of the epitaxial overgrowth on the $\{111\}$ B substrate. Laue photographs of the sample shown in Figure 10(B) were taken to display the evidence of the epitaxy. The Laue photograph of the substrate indicated

a single crystal with the {111} crystallographic orientation. The Laue photograph of the overgrowth displayed an identical pattern thus confirming the epitaxy.

The initial conditions of the system control the surface rates of the samples. The initially introduced amount of the ammonium chloride controls the etching rate of the source and the deposition rate of the seed. The etching rate and the deposition rate of the samples are shown in Figure 11 and 12 as a function of the initially introduced amount of the ammonium chloride. The source wafers in Figure 11 were the p-type, zinc-doped polycrystalline gallium arsenide, and the seed wafers were the n-type, Te-doped, {111} B single crystal gallium arsenide. The surfaces of the source and the seed were chemically polished. Such parameters as the separation distance, d, the temperature difference, ΔT, and the average temperature, T_{av}, were kept constant for the series of runs. No excess arsenic was used. The source wafers in Figure 12 were the n-type, Te-doped, {110} single crystal gallium arsenide, and the seed wafers were the p-type, zinc-doped, {110} single crystal gallium arsenide. Other parameters such as <As> b, ΔT, T_{av}, and the surface conditions were kept constant for the series. The deposition rate on the seed in general decreases with the increasing initial amount of the amonium chloride. The etching rate of the source follows closely the trend of the deposition rate.

The non-stoichiometric excess arsenic initially introduced in the system also affects the rates of deposition and etching of the sample. In Figure 13 the rates of deposition and etching of the source are shown to be dependent on the excess arsenic initially introduced.

Experimental Studies of Growth Characteristics

Studies of the growth surfaces showed orange-peel type growth on {110} seeds at 10^{-5} gr/cm^2 sec. and mirror-like growth at 1.35×10^{-5} gr/cm^2 sec. Dislocations visibly alter the growth. Other factors may have been more important in the growth characteristic than the growth rate, which was not readily controlled. Typical surface patterns of the epitaxial overgrowth on {100} substrates are shown in Figure 14. Figure 14a and 14b exhibit the smooth

surface growth with the dislocation growth patterns. The dislocation growth pattern on {100} surface resembles the circular cone. Figure 14c is a typical photomicrograph of such a circular cone with apparent singularity of its apex. When two or more circular cones emerge together rendering more than one apex, the configuration of the cone structure appears as having a characteristic spiral pattern on top as shown in Figure 14d and 14e. Smooth epitaxial overgrowth on {111} A seed surface and the etched pattern of the {111} A source surface are shown in Figure 15a. A typical pattern of the epitaxial growth on {111} B seed surface, and an etched pattern of the {111} B source surface are shown in Figure 15b. The tetrahedral pyramid patterns of protrusions on the seed surface and of etch pits on the source surface are shown in Figures 15c, 15d, 15e, and 15f. The tetrahedral pyramid with one apex is shown in Figure 15c. Spiral patterns are observed in Figures 15d and 15e with merging of two or more apexes in a pyramid. The etch pit pattern shown in Figure 15f resembles that of the tetrahedral pyramid protrusion. The characteristic spiral etch pit observed here contains several apexes within itself. The characteristic growth patterns at the dislocations observed exhibit unique identifications to the crystallographic orientation of the substrate.

It is possible to obtain very high deposition rates if the crystallographic perfection of the epitaxially grown layer is disregarded. For example, when the rate of the impinging flux on the surface of the seed is far greater than the rate at which the atoms can add on perfectly, the deposited materal will probably form stacking faults as these do not have a very high energy, and this accomodates the greater flux. The resultant deposition rate may be very high compared with the rate for "perfect" epitaxial growth. Figure 16a exhibits the stacking faults observed on {111} B seed surface. The density of the stacking faults can be so great that the grown layer can probably no longer be catagorized as a single crystal.

The rate of the "perfect" epitaxial growth differs for the crystallographic orientation of the substrate on which the epi-

taxial overgrowth is attempted. The comparison of the rates of the "perfect" epitaxial growth (stacking faults not readily observed) listed in Table #VI shows that the rates on the low index orientation appears to be {110} > {100} > {111}B > {111}A. In order to determine whether the relation {100} > {111}B was good, experiments were conducted using {111}B seed and {100} source, and vice versa. It is assumed that, if the impinging flux at the growth surface would exceed the maximum rate of the "perfect" epitaxial growth of the surface, there would be stacking faults formed. Figure 17a shows the case of the {111}B seed and the {100} source, which supplied the impinging flux to the {111}B seed, obviously exceeding the "perfect" epitaxial growth rate of the {111}B seed. Hence, the high density of stacking faults are formed on the {111}B seed surface. The opposite arrangement of the {100} seed and the {111}B source renders the result shown in Figure 17. The etching rate of the {111}B source apparently was less than the "perfect" epitaxial growth rate of the {100} seed. The result shows stacking fault-free nucleation and growth. From the above observations, it is concluded that the "perfect" epitaxial growth rate of the {100} orientation is greater than that of {111}B. A corollary involves a growth imaging effect which occurs by having the separation spacing between the seed and the source wafers very small, and having the source a bicrystal with two very different etch rates. When the image-growth is on the {100} seed and the source orientation for one portion has a {111}A and almost any other orientation for the other portion a very much greater growth takes place where the etching is faster. This result also indicates that the lateral dispersion of the molecules transported between the seed and the source is very small.

The structural patterns of the early stage of the growth on the low index crystallographic orientations indicate definite correlation between the growth pattern and the substrate orientation. Islands of often truncated triangular based structures are shown in Figure 18. The islands grown on the {111}A surface resemble tetrahedral pyramids. On the {111}B surface the structural pattern has truncated triangular base and truncated pyramidal apex. If the growth structure of a twinned island merges to the

island with the "perfect" epitaxial growth, there will be a twin boundary between the two islands as shown in Figure 18c.

The island structures on {100} surface are rectangular based and truncated roof-top as shown in Figure 19. Frequently the truncated rectangular base was observed as shown in Figure 19a. When the island structures grow large enough, the dislocation growth patterns become apparent on the surface of the overgrowth. An early stage of epitaxial growth on a {110} surface is shown in Figure 20. The structures resemble rectangular based "roof-top" and the base is often truncated at the corners.

A typical example of the epitaxial overgrowth on {111} B seed using ammonium iodide as the transporting material is shown in Figure 21. Although extensive efforts to obtain a "perfect" epitaxial growth were not made using ammonium bromide, it was possible to obtain rough growths with the high density of stacking faults in two trial runs.

Interface Studies

The interface between the substrate and the epitaxial grown layer were examined by photomicrographic observations of the cross-sectional surface, which was cleaved and etched in the Schell etch (HNO_3 : H_2O :: 1 : 2) for 90 seconds. When a p-type substrate and a n-type source or vice versa are used p-n junction results. If the effect of diffusion is negligible during the growth process and no substrate etching takes place, the p-n junction should coincide with the interface. The interfaces and/or the p-n junctions produced by several techniques, "large-separation" epitaxial growth, "close-spaced" epitaxial growth, impurity diffusion, solution growth techniques, are compared. The interfaces were examined in cross-section obtained by {110} cleaving. The one sample was grown by the horizontal vapor transport technique in a closed-system having the large-separation ($\simeq$ 8 cm.) between the source and the seed. NH_4Cl was the transport agent. P-type layers were grown on the chemically polished n-type surface. Both {111} B and {111} A surfaces were used as substrate. The interfaces and hence the p-n junctions were irregular and non-planar. An extensive effort was made to produce a flat and

abrupt p-n junction with the "close-spaced" epitaxial growth technique. Some typical examples of the interfaces and/or the p-n junctions produced by the "close-spaced" technique are shown in Figure 22, which shows the cleaved and etched {110} cross-section of the sample which was produced by growing p-type layer on the n-type substrate. The transporting agent was the ammonium iodide (NH_4I) and some elemental zinc was also introduced to dope the epitaxially grown layer. The {111} B substrate was chemically polished. The effect of zinc diffusion is observed when Zn is in the source. The epitaxially grown layer in Figure 22c was Te-doped (n-type) and the substrate is zinc-doped (p-type). No visible diffusion effect is observed for this sample: the interface coincides with the p-n junction. All of the junctions were flat and no interfacial irregularities are observed.

V. CONCLUSION

The usefullness of the ammonium halides as transporting agents in epitaxial vapor growth techniques is demonstrated in Section IV. It is important not to exceed the maximum rate of the "perfect" epitaxial growth. Excessive density of the stacking faults is a frequent result of the rapid rate of growth. The rates of the growth of facets predicted from the "atomistic" model proposed by Faust and John[1] are in good agreement with our rate-limited experimental results which are {110} > {100} > {111} B > {111} A. The "island" structures of epitaxial growth with the definite crystallographic facets constructed by the "atomistic" stacking arrangements resembles our experimental observations.

Similar observations of the definite crystallographic facets were produced by the dissolution and redeposition of semiconductors in molten metals and reported by Faust, Sagar, and John[1].

REFERENCES

1. J. W. Faust, Jr. and H. F. John, "Growth Facets on III-V Intermetallic Compounds", J. Phys. Chem. Solids, 23, pp. 1119-1122, (1962).

2. O. Kubaschewski and E. L. Evans, "Metallurgical Thermochemistry", Pergamon Press, (1958).

3. K. K. Kelley, Bureau of Mines Bulletin #584, #592, U. S. Government Printing Office, Washington, D. C., (1961).

4. B. J. McBride and et. al., "Thermodynamic Properties to 6000°K for 210 Substances Involving the First 18 Elements", NASA SP-3001, Washington, D. C., (1963).

5. D. R. Stull and G. C. Sinke, "Thermodynamic Properties of the Elements", American Chemical Society, (1956).

6. D. R. Stull, et. al.: JANAF Thermochemical Tables. The Dow Chem. Co., Midland, Mich., Dec. 31, 1960 - Sept. 30, 1962.

7. F. R. Bichowsky, Data on Chemical Thermodynamics (Book).

8. W. M. Latimer, "Methods of Estimating the Entropies of Solid Compounds", J. Am. Chem. Soc., 73, 1480 (1951).

9. R. R. Fergusson and T. Gabor, "The Transport of Gallium Arsenide in the Vapor Phase by Chemical Reaction", J. of Electrochemical Society, Vol. 3, No. 5, pp. 585-592, (May, 1964).

10. J. W. Faust, Jr., A. Sagar, and H. F. John, "Molten Metal Etches for the Orientation of Semiconductors by Optical Techniques", J. Electrochemical Soc. 109, pp. 824-828, (Sept., 1962).

11. R. F. Lever and G. Mandel, "Diffusion and the Vapor Transport of Solids", J. Phys. Chem. Solids V. 23, pp. 599-600, (1962).

12. R. F. Lever, "Multiple Reaction Vapor Transport of Solids", J. of Chem. Phys. V. 37, No. 5, pp. 1078-1081, (Sept., 1962).

Table I

Reaction Equations (all components are gas phase except GaAs)

$$\left(\tfrac{1}{2}\right)H_2 + \left(\tfrac{1}{2}\right)Cl_2 \rightleftharpoons HCl \quad (1)$$

$$\left(\tfrac{1}{2}\right)N_2 + \left(\tfrac{3}{2}\right)H_2 \rightleftharpoons NH_3 \quad (2)$$

$$NH_3 + HCl \rightleftharpoons NH_4Cl \quad (3)$$

$$GaCl + Cl_2 \rightleftharpoons GaCl_3 \quad (4)$$

$$GaAs(s) + \left(\tfrac{1}{2}\right)Cl_2 \rightleftharpoons GaCl + \left(\tfrac{1}{4}\right)As_4 \quad (5)$$

$$\left(\tfrac{1}{4}\right)As_4 + \left(\tfrac{3}{2}\right)Cl_2 \rightleftharpoons AsCl_3 \quad (6)$$

Equilibrium Constants

$$K_1(T) = [HCl]\,[H_2]^{-1/2}[Cl_2]^{-1/2} \quad (7)$$

$$K_2(T) = [NH_3]\,[N_2]^{-1/2}[H_2]^{-3/2} \quad (8)$$

$$K_3(T) = [NH_4Cl]\,[NH_3]^{-1}[HCl]^{-1} \quad (9)$$

$$K_4(T) = [GaCl_3]\,[GaCl]^{-1}[Cl_2]^{-1} \quad (10)$$

$$K_5(T) = [GaCl]\,[As_4]^{1/4}[Cl_2]^{-1/2} \quad (11)$$

$$K_6(T) = [AsCl_3]\,[As_4]^{-1/4}[Cl_2]^{-3/2} \quad (12)$$

Table II

Conservative Equations

$$\boxed{Cl_2} = \tfrac{3}{2}[GaCl_3] + \tfrac{1}{2}[GaCl] + [Cl_2] + \tfrac{1}{2}[HCl] + \tfrac{1}{2}[NH_4Cl] + \tfrac{3}{2}[AsCl_3] \quad (13)$$

$$\boxed{H_2} = [H_2] + \tfrac{3}{2}[NH_3] + 2[NH_4Cl] + \tfrac{1}{2}[HCl] \quad (14)$$

$$\boxed{N_2} = [N_2] + \tfrac{1}{2}[NH_3] + \tfrac{1}{2}[NH_4Cl] \quad (15)$$

$$\boxed{As} = 4[As_4] + [AsCl_3] + GaAs\ (solid) \quad (16)$$

$$\boxed{Ga} = [GaCl] + [GaCl_3] + GaAs\ (solid) \quad (17)$$

$$\boxed{As} - \boxed{Ga} = 4[As_4] + [AsCl_3] - [GaCl] - [GaCl_3] = \langle As \rangle = -\langle Ga \rangle \quad (18)$$

Table III

Species	$H_T = aT + bT^2 + cT^{-1} + d$ ($\frac{cal}{mole}$)	H_{298} ($\frac{kcal}{mole}$)	Ref. #
H_2	$6.52T + 0.39 \times 10^{-3}T^2 - 0.12 \times 10^{5}T^{-1} - 1938$	0	3,4
N_2	$6.83T + 0.45 \times 10^{-3}T^2 + 0.12 \times 10^{5}T^{-1} - 2117$	0	3,4
Cl_2	$8.85T + 0.08 \times 10^{-3}T^2 + 0.68 \times 10^{5}T^{-1} - 2874$	0	3,4
NH_3	$7.11T + 3. \times 10^{-3}T^2 + 0.37 \times 10^{5}T^{-1} - 13541$	-11.03	3,4
HCl	$6.27T + 0.62 \times 10^{-3}T^2 - 0.3 \times 10^{5}T^{-1} - 23887$	-22.063	3,2,4
NH_4Cl	$30T - 53431$	-42.4	6,7,8
As_4	$19.84T + 1.2 \times 10^{5}T^{-1} + 28182$	34.5	3,5
As_2	$8.93T + 0.52 \times 10^{5}T^{-1} + 45163$	48.	3,5
$AsCl_3$	$19.72T + 0.05 \times 10^{-3}T^2 + 1.46 \times 10^{5}T^{-1} - 77874$	-71.5	3,9
GaCl	$8.93T + 0.38 \times 10^{5}T^{-1} - 18990$	-16.2	3,9
$GaCl_3$	$19.2T - 107700$	-125	9
GaAs (s)	$12.0T - 21600$	-18.5	9

Table IV

Species	$S_T = a\ln T + bT + cT^{-2} + d$ (e.u.) $\frac{cal}{mol.\ deg.}$	S_{298}(e.u.)	Ref. #
H_2	$6.52\ln T + 0.78 \times 10^{-3} T - 0.06 \times 10^{5} T^{-2} - 6.1159$	31.2	3,9,4
N_2	$6.83\ln T + 0.9 \times 10^{-3} T + 0.06 \times 10^{5} T^{-2} + 6.5243$	45.771	3,4
Cl_2	$8.85\ln T + 0.16 \times 10^{-3} T + 0.34 \times 10^{5} T^{-2} + 2.4202$	53.291	3,4
NH_3	$7.11\ln T + 6 \times 10^{-3} T + 0.185 \times 10^{5} T^{-2} + 3.121$	46.045	3,4
HCl	$6.27\ln T + 1.24 \times 10^{-3} T - 0.15 \times 10^{5} T^{-2} + 8.7222$	44.646	3,2,4
NH_4Cl	$30\ln T - 87.924$	89.986	6,8,7
As_4	$19.84\ln T + 0.6 \times 10^{5} T^{-2}$ 038.675	75.0	3,5
As_2	$8.93\ln T + 0.26 \times 10^{5} T^{-2} - 6.0025$	57.19	3,5
$AsCl_3$	$19.72\ln T + 0.1 \times 10^{-3} T + 0.73 \times 10^{5} T^{-2} - 34.269$	78.2	3,9
GaCl	$8.93\ln T + 0.19 \times 10^{5} T^{-2} + 5.274$	56.4	3,9
$GaCl_3$	$19.17\ln T - 29.3$	79.7	9
GaAs (s)	$11.96\ln T + 1.6 \times 10^{-3} T - 53$	15.6	9

Table V

Reactions	$\ln K = -\frac{\Delta F}{RT}$	
	$\Delta F/T = A \ln T + BT + CT^{-2} + DT^{-1} + E$	ΔF_{1000} ($\frac{kcal}{mole}$)
$\frac{1}{2}H_2 + \frac{1}{2}Cl_2 \rightleftharpoons HCl$	$1.415 \ln T - 0.385 \times 10^{-3} T - 0.29 \times 10^{5} T^{-2} - 2148.1 T^{-1} - 11.9851$	-24.1039
$\frac{1}{2}N_2 + \frac{3}{2}H_2 \rightleftharpoons NH_3$	$6.085 \ln T - 2.19 \times 10^{-3} T + 0.245 \times 10^{5} T^{-2} - 9575.5 T^{-1} - 15.1177$	15.1581
$NH_3 + HCl \rightleftharpoons NH_4Cl$	$-16.62 \ln T + 3.62 \times 10^{-3} T - 0.035 \times 10^{5} T^{-2} - 16003 T^{-1} + 116.3872$	-10.827
$GaCl + Cl_2 \rightleftharpoons GaCl_3$	$-1.39 \ln T + 0.08 \times 10^{-3} T - 0.53 \times 10^{5} T^{-2} - 85836 T^{-1} + 38.4142$	-56.9983
$GaAs + \frac{1}{2}Cl_2 \rightleftharpoons GaCl + \frac{1}{4}As_4$	$2.495 \ln T + 1.64 \times 10^{-3} T + 0.17 \times 10^{5} T^{-2} + 11092.5 T^{-1} - 49.84$	-19.81
$\frac{1}{4}As_4 + \frac{3}{2}Cl_2 \rightleftharpoons AsCl_3$	$-1.485 \ln T + 0.07 \times 10^{-3} T + 0.07 \times 10^{5} T^{-2} - 80608.5 T^{-1} + 29.7155$	-61.075

Table VI

Seed	Source	t(hrs.)	Deposition Rate R_g (gr/cm^{2}sec)	Etch Rate R_e (gr/cm^{2}sec)
X-48 {111} A	X-33 {111} A	2	1.36×10^{-6}	-3.23×10^{-6}
X-48 {111} A	X-33 {111} A	2	$.607 \times 10^{-6}$	-2.77×10^{-6}
X-48* {111} A	X-33** {111} A	2	$.914 \times 10^{-6}$	-3.03×10^{-6}
X-48 {111} B	X-33 {111} B	2	1.947×10^{-6}	-4.0×10^{-6}
X-48 {100}	X-33 {100}	2	1.655×10^{-6}	-3.88×10^{-6}
X-48 {100}	X-33 {100}	3	3.26×10^{-6}	-8.43×10^{-6}
X-48 {110}	X-33 {110}	2	9.74×10^{-6}	-11.27×10^{-6}

* Mechanical Polish

** Chemical Polish

T = 693°C

$[NH_4Cl]$ = 5 mg.

$\langle As \rangle = 0$

Area = .8 cm^2

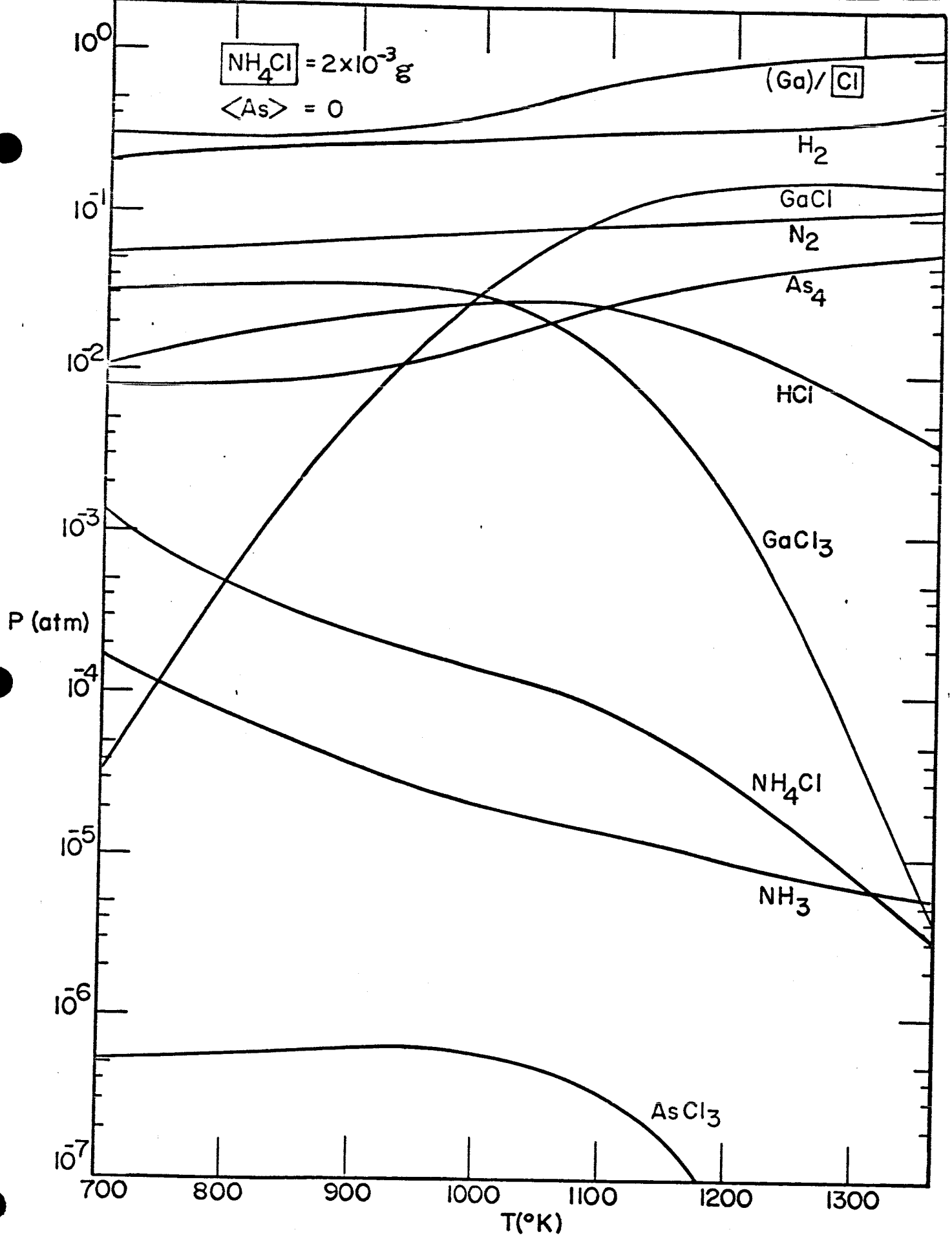

Figure 1. Composition of the gas phase of NH_4Cl–Gals system vs. temperature with the initial values of (Ga)/Cl = 2 mg. and no excess arsenic.

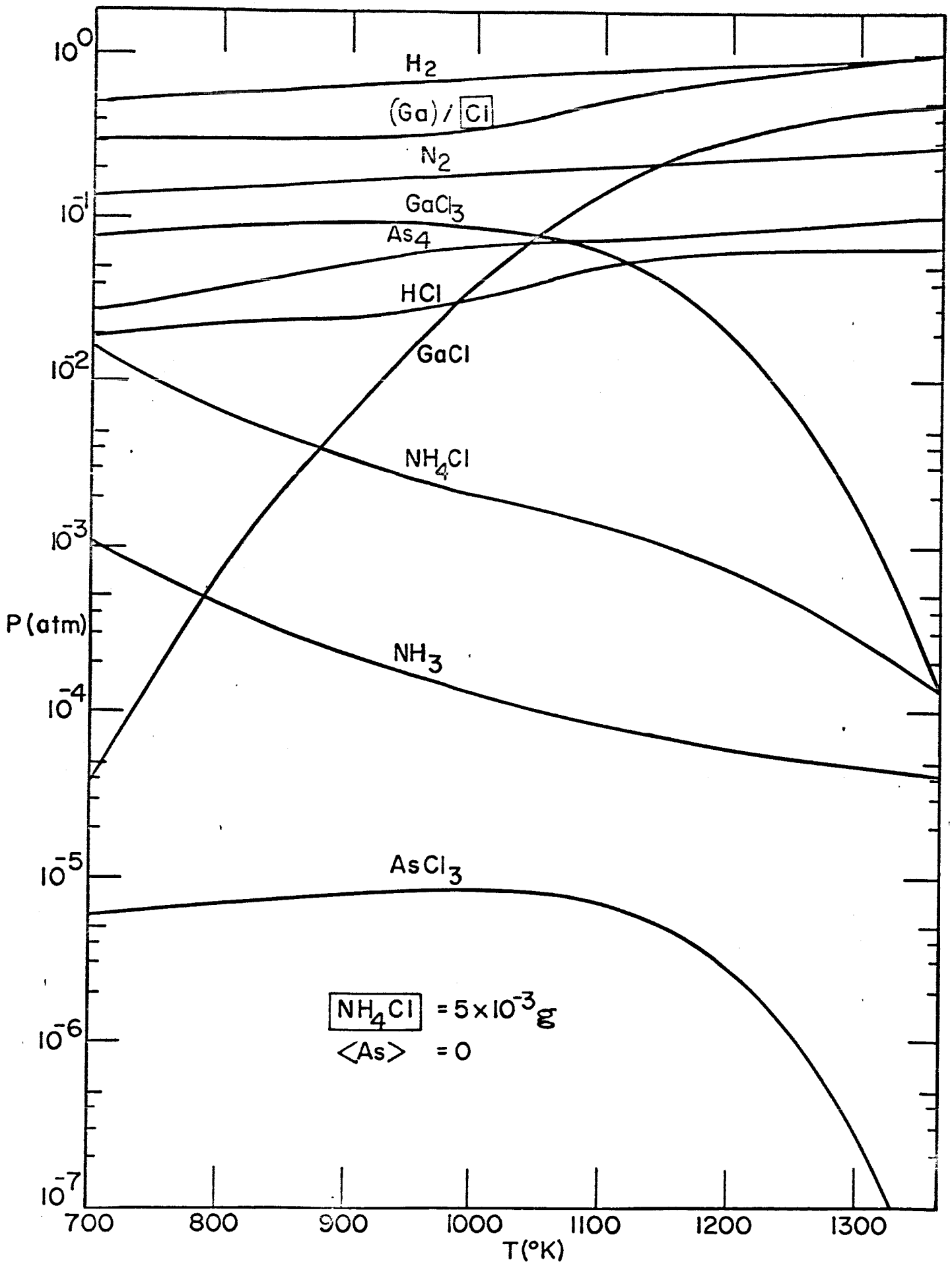

Figure 2. Composition of the gas phase of NH4Cl-GaAs system vs. temperature with the initial values of NH4Cl = 5 mg. and no excess arsenic.

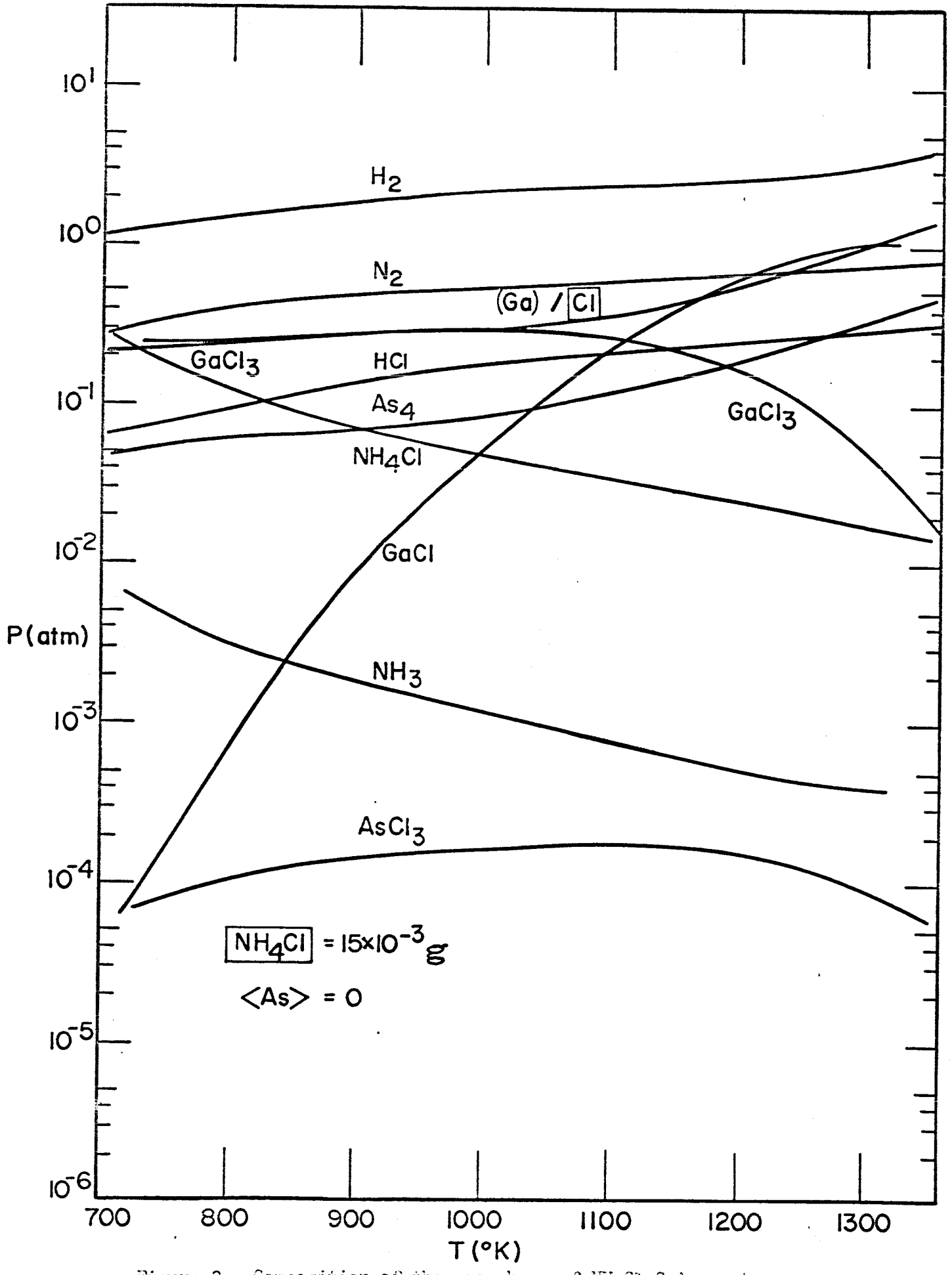

Figure 3. Composition of the gas phase of NH_4Cl–GaAs system vs. temperature with the initial values of NH_4Cl = 15 mg. and no excess arsenic.

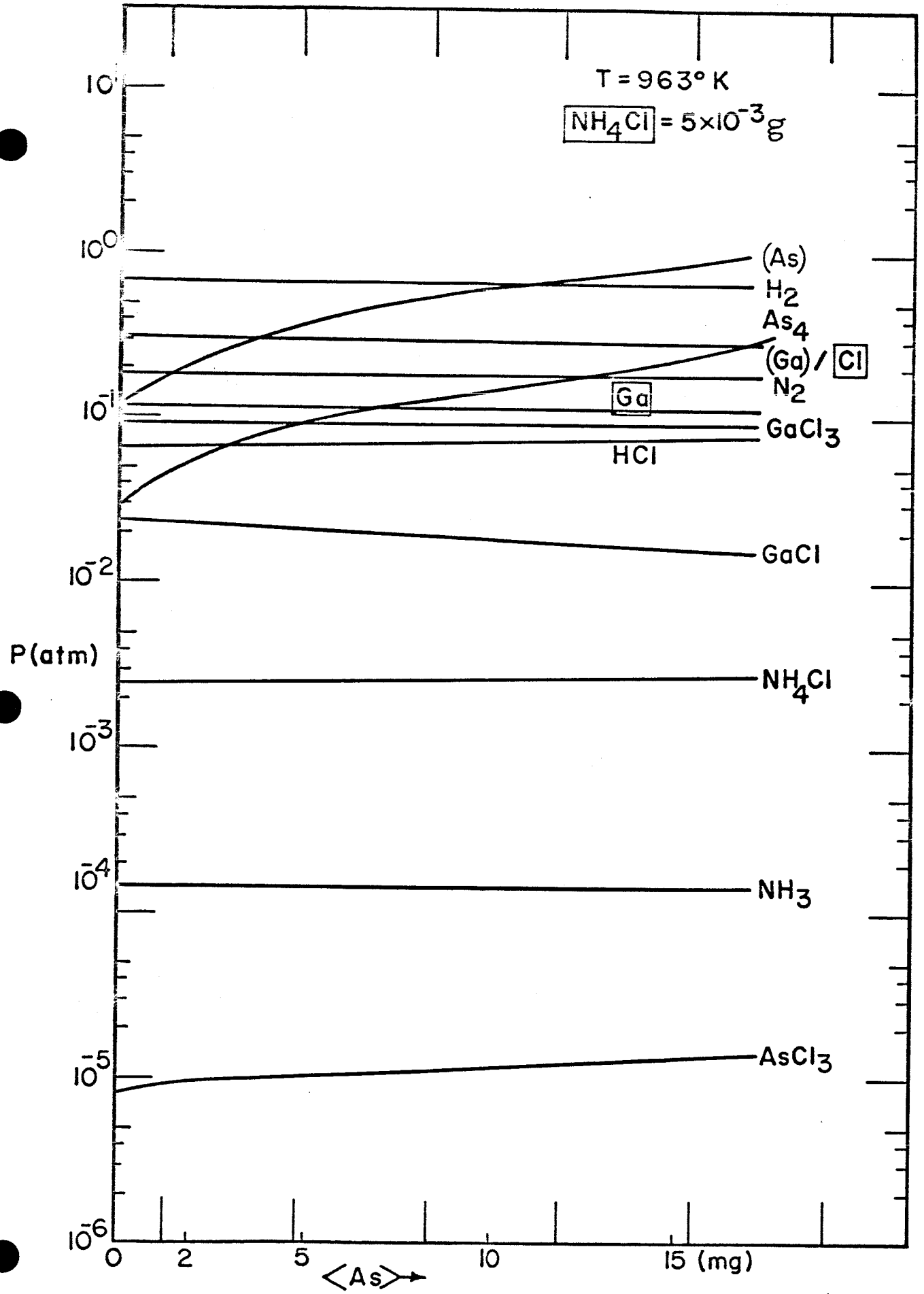

Figure 4. Composition of [illegible] vs. <As> at T = 963°K and [illegible] = 5 mg.

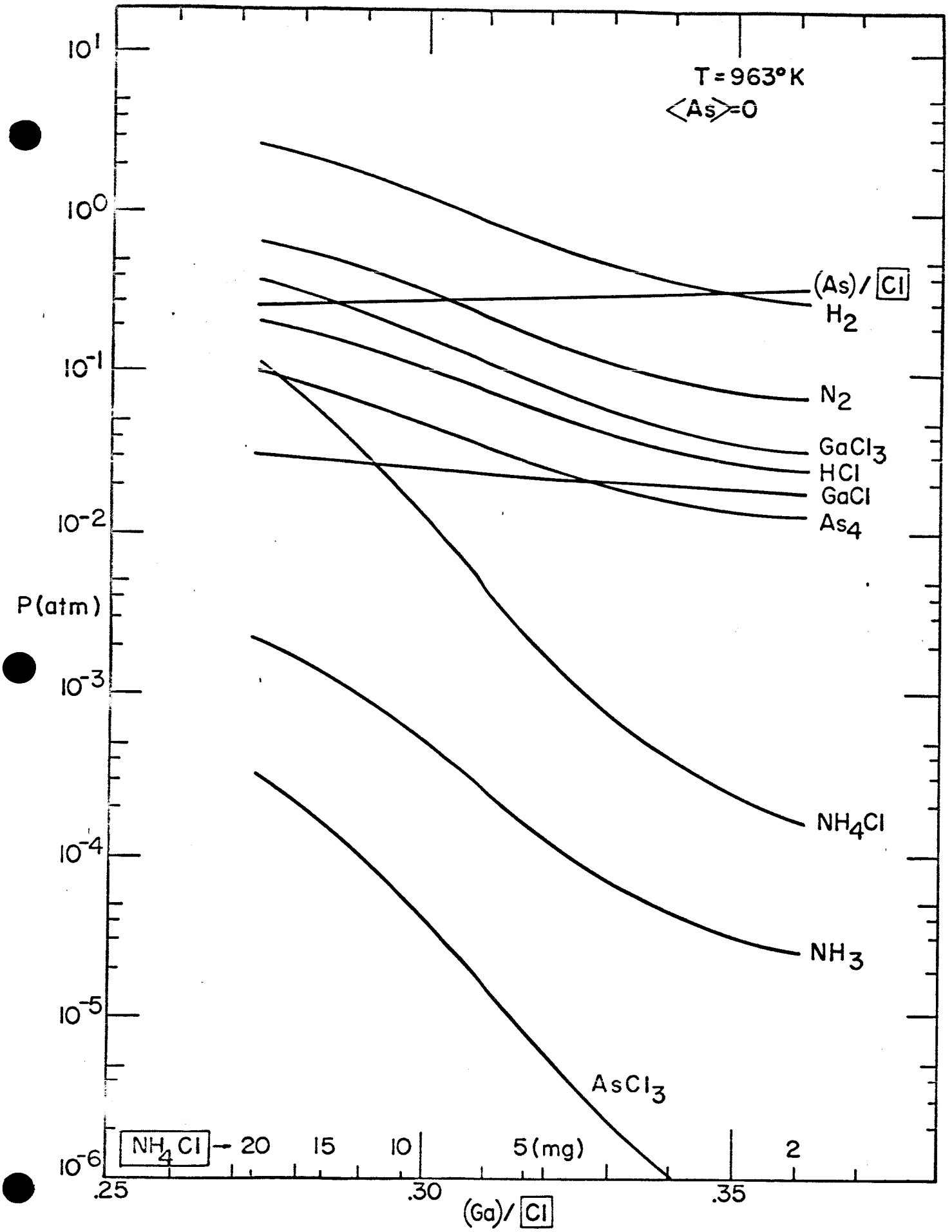

Figure 5. Composition of the gas phase vs. the [illegible] ratio (As) / Cl and Cl / Ga at T = 963°K and no excess arsenic.

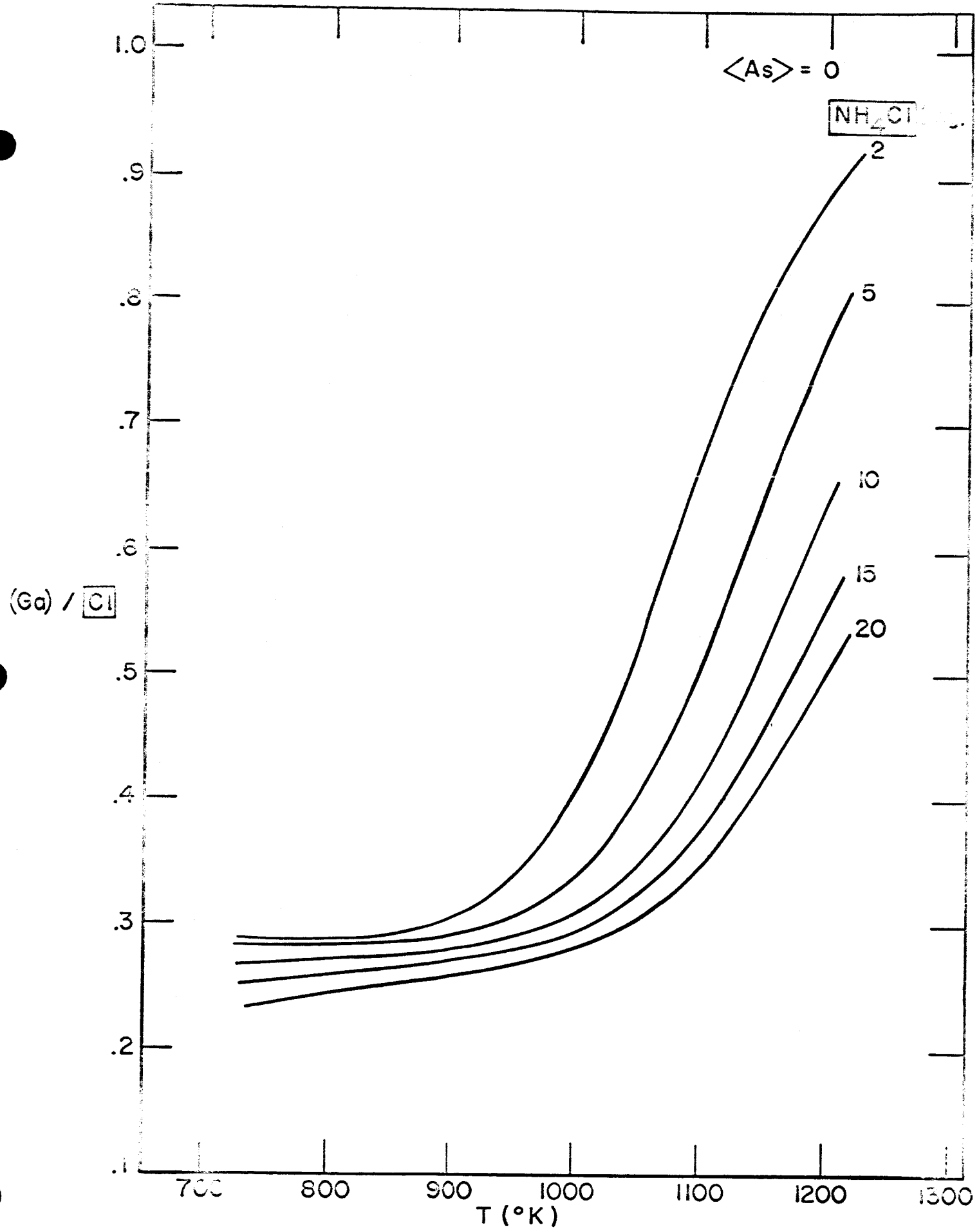
1.0
.9
.8
.7
.6
.5
.4
.3
.2
.1
(Ga) / Cl
<As> = 0
NH4Cl
2
5
10
15
20
700
800
900
1000
1100
1200
1300
T (°K)

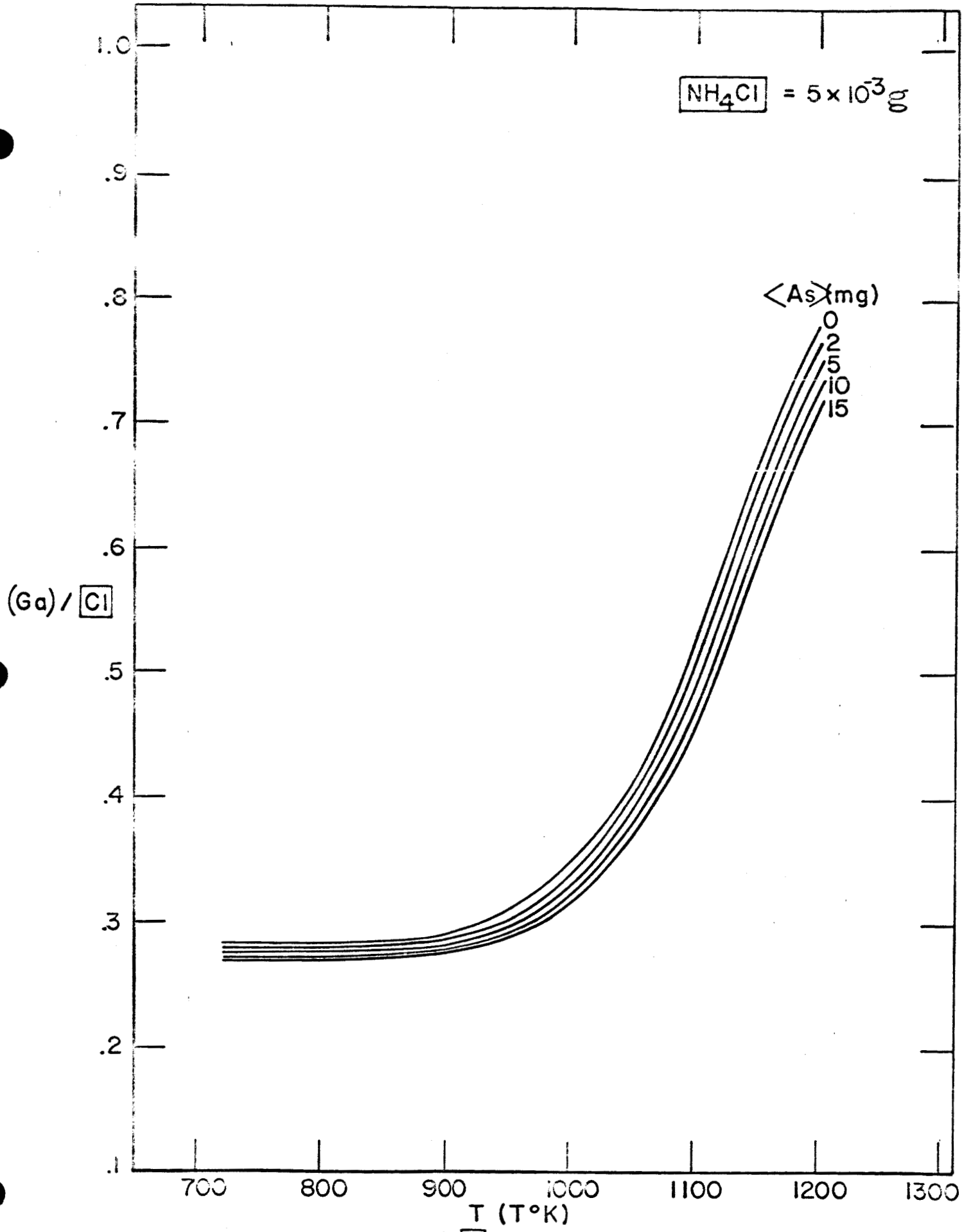

Figure 7. Component (Ga)/ Cl vs. temperature with various initial values of <As> and at m_{NH_4Cl} = 5 mg.

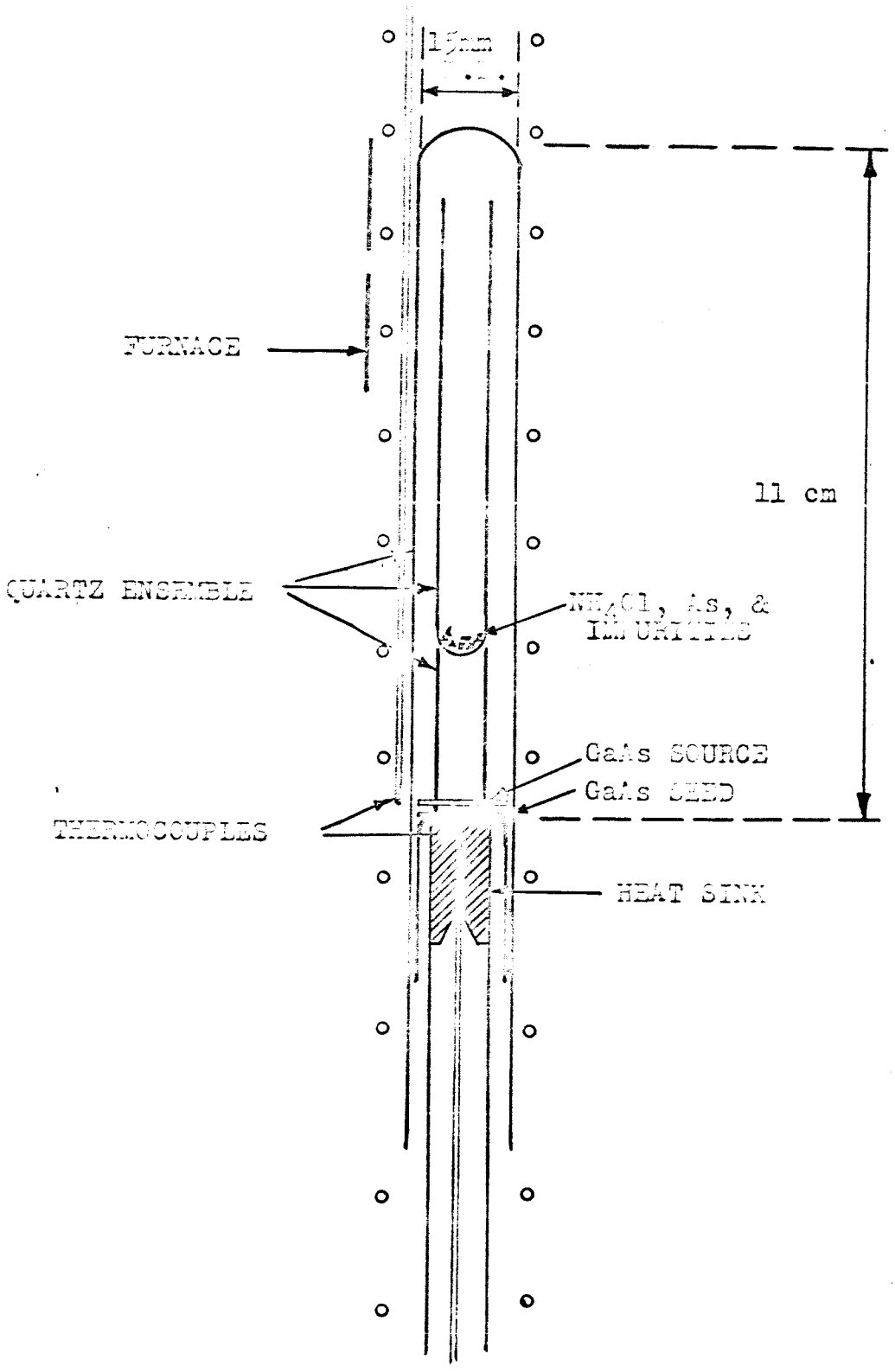

Figure 8. Vertical reaction tube configuration for "close-spaced" deposition of gallium arsenide.

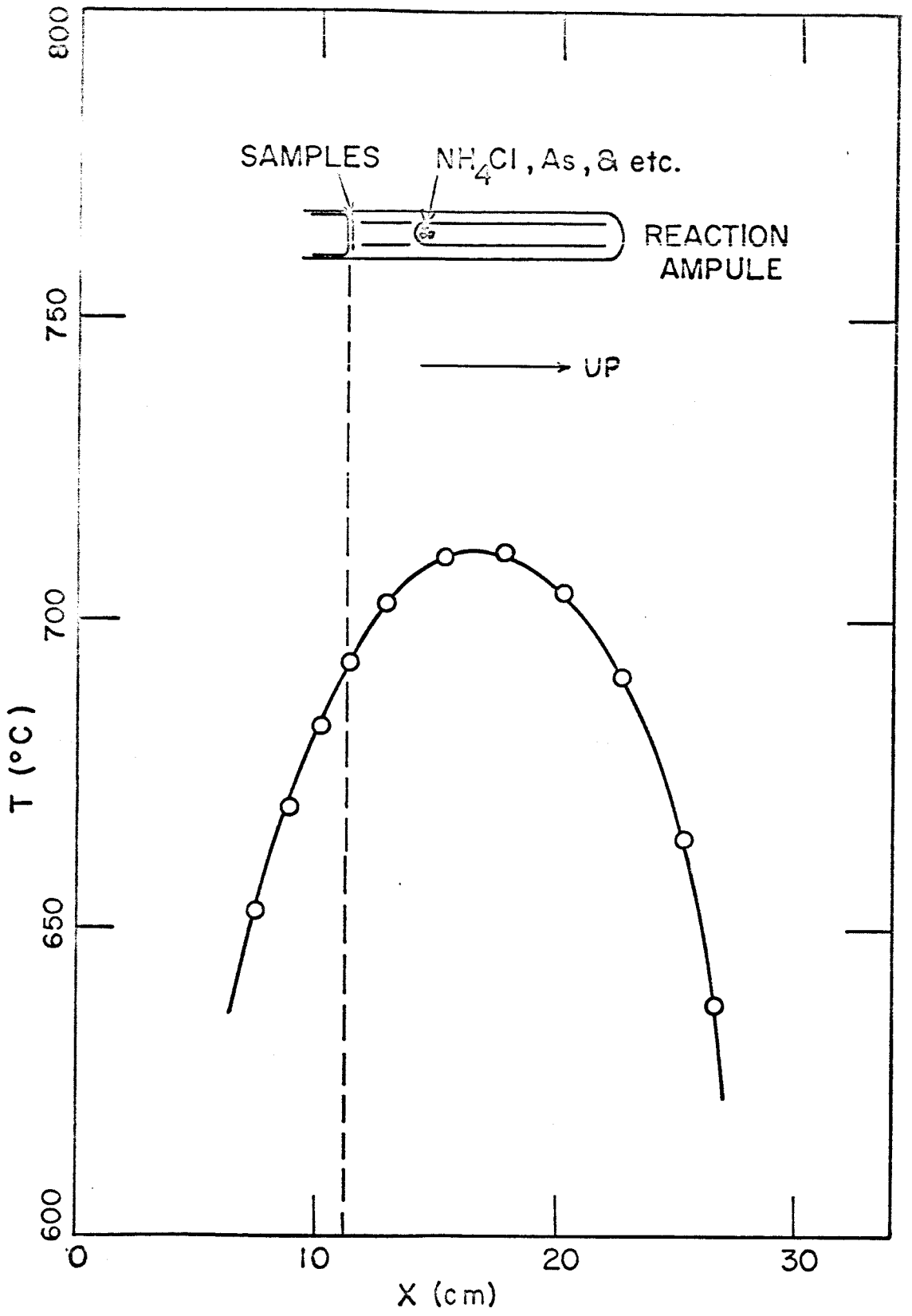
SAMPLES
NH_4Cl, As, & etc.
REACTION AMPULE
UP
T (°C)
800
750
700
650
600
0
10
20
30
X (cm)

Figure 9. [illegible]

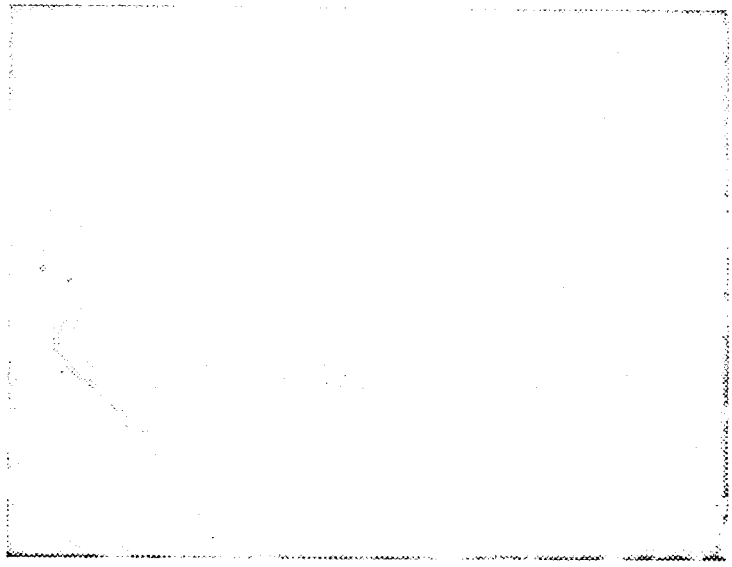

(a)

Polycrystalline seed

2 mm

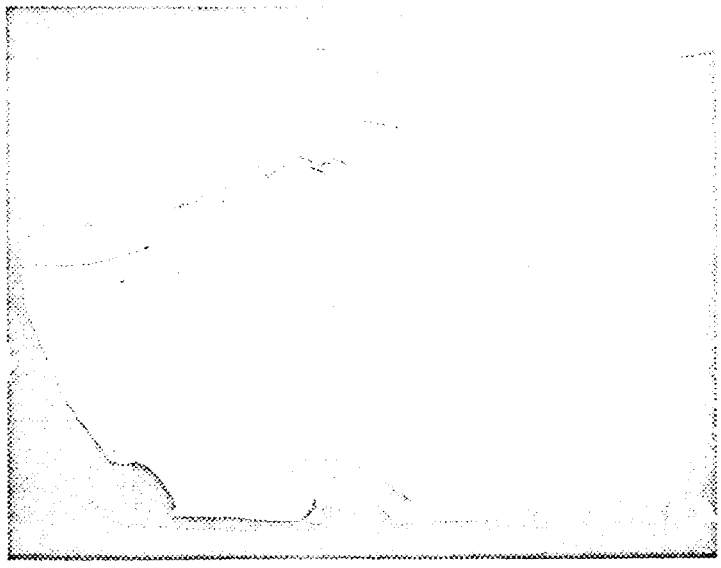

(b)

Figure 10. Epitaxial overgrowth (a) on polycrystalline seed and (b) on {111} B single crystal seed.

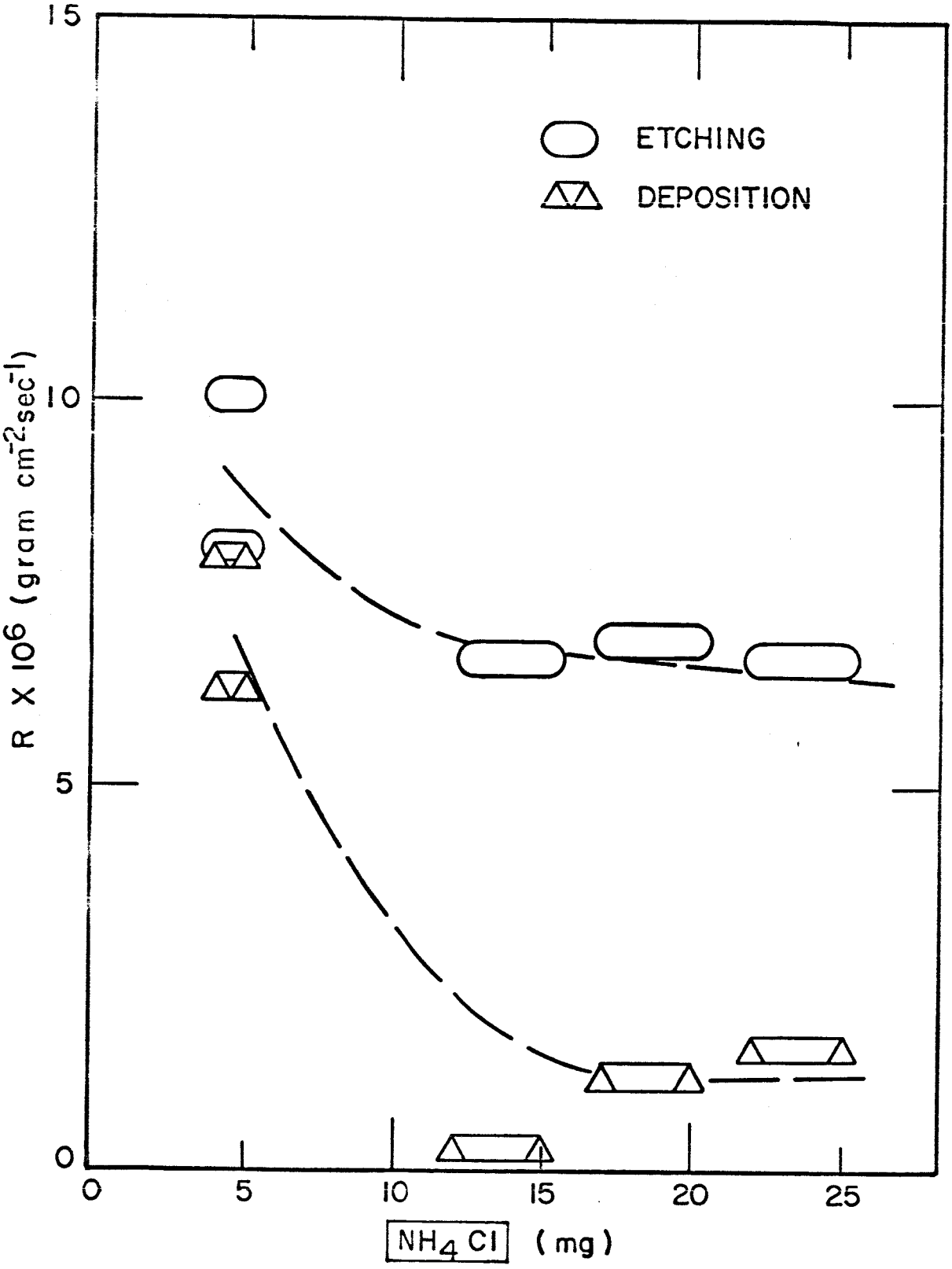

Figure 11. Rates of deposition on the {111}A surface and etching of the GaAs epitaxial source vs. the initial values of [illegible] at T = 675°C and <As> = 0.

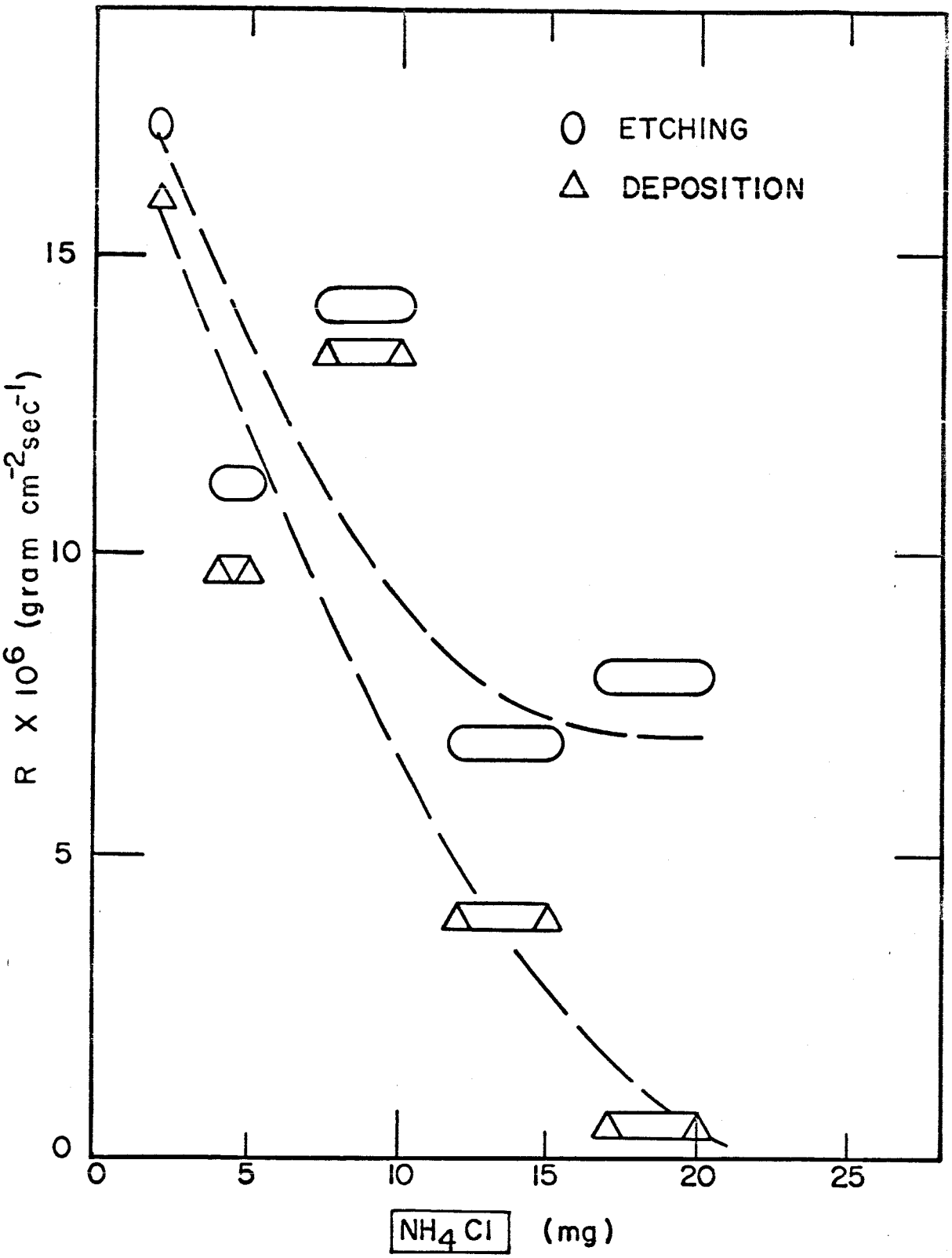

Figure 12. Rates of deposition on the {110} [illegible] of the {110} centres vs. the initial values of [illegible] at T = [illegible] and <ia> = 0.

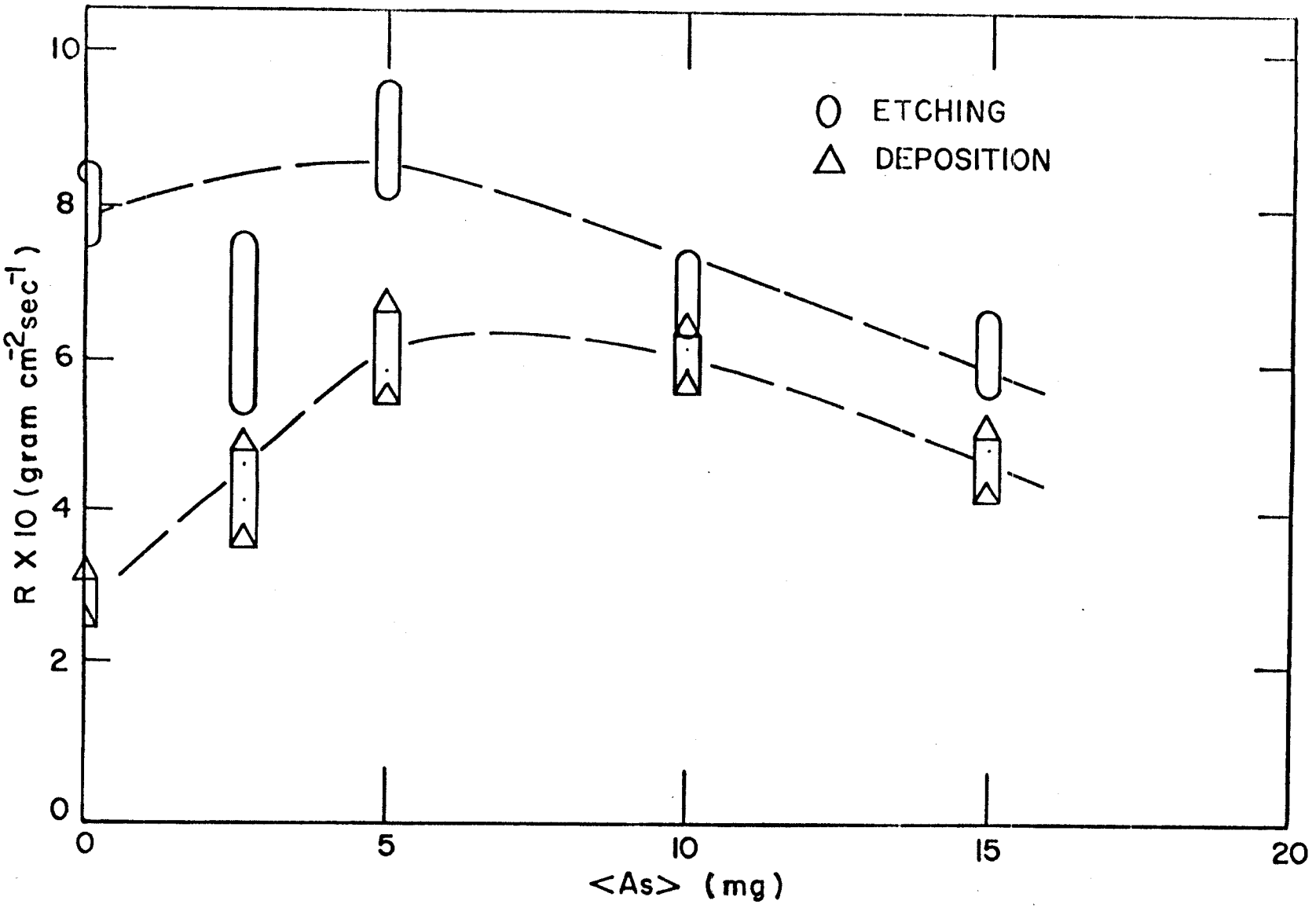

Figure 13. Rates of deposition on the {100} seed and etching of the {100} source vs. the initial values of <As> at $[NH_4Cl]$ = 5 mg. and T = 966°K.

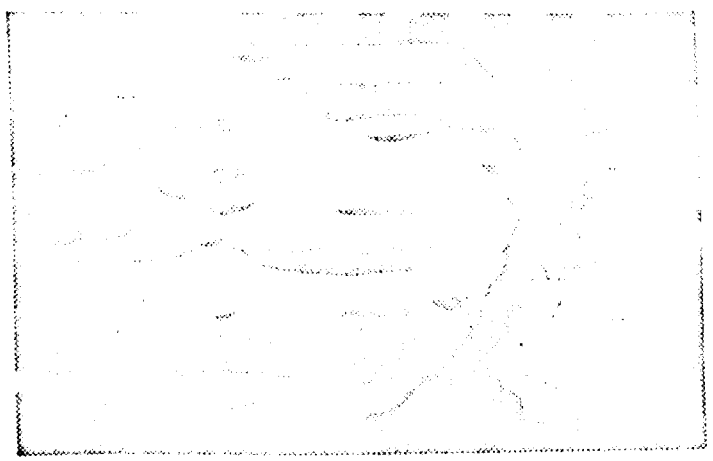

2mm

(a)

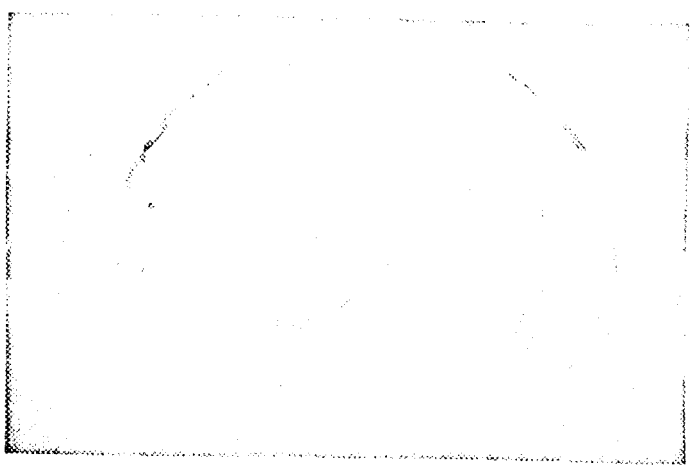

2mm

(b)

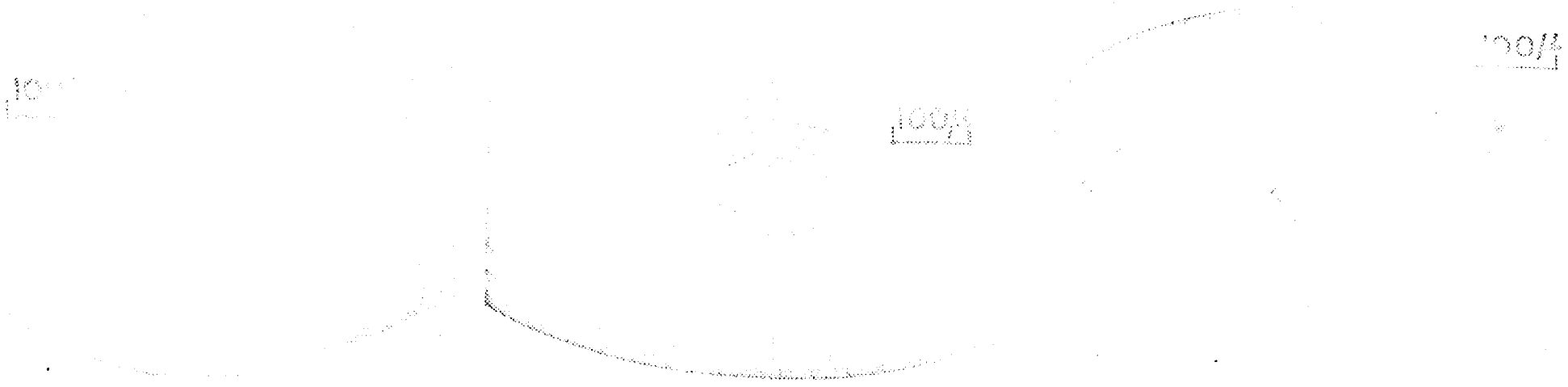

(c) 66x

(d) 66x

(e) 66x

Figure 14. Photomicrographs of the epitaxial overgrowth on {100} seed surface. (a) Surface pattern with many dislocation-growths, and $R_s = 3.26 \times 10^{-6}$ gr $cm^{-2} sec^{-1}$. (b) Surface pattern with many dislocation-growths, and $R_s = 4.88 \times 10^{-6}$ gr $cm^{-2} sec^{-1}$. (c) A dislocation-growth of the circular cone with one apex. (d) and (e) Dislocation-growth of the circular cone with multiple apexes showing spiral structures.

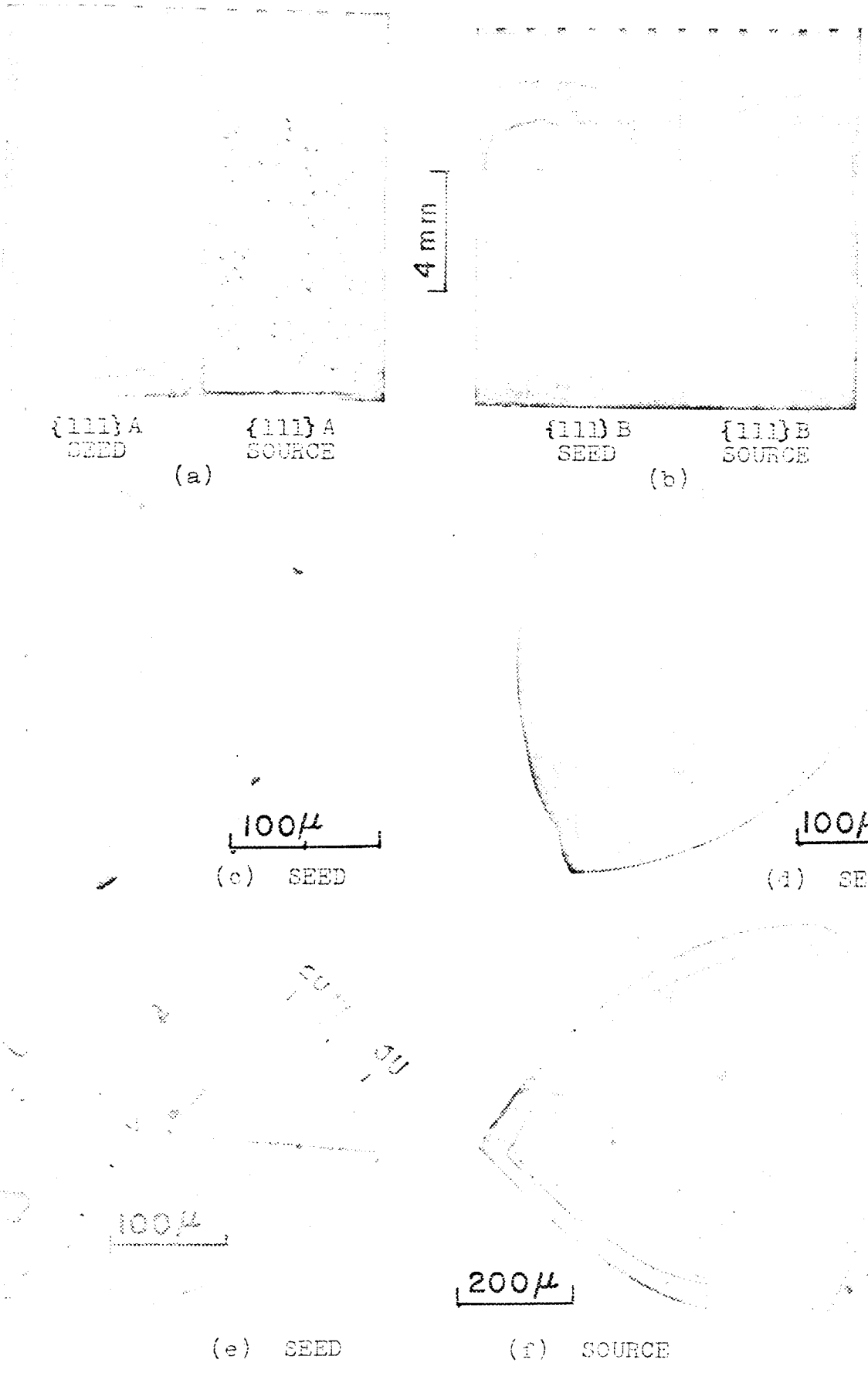

Figure 15. Photomicrographs of the epitaxial overgrowth pattern of the seed and the etched surface pattern of the source. (a) {111} A seed and {111} A source. (b) {111} B seed and {111} B source. (c) Tetrahedral dislocation-growth with one apex. (d) and (e) Tetrahedral dislocation-growth with multiple apexes. (f) Tetrahedral etch-pit with multiple apexes.

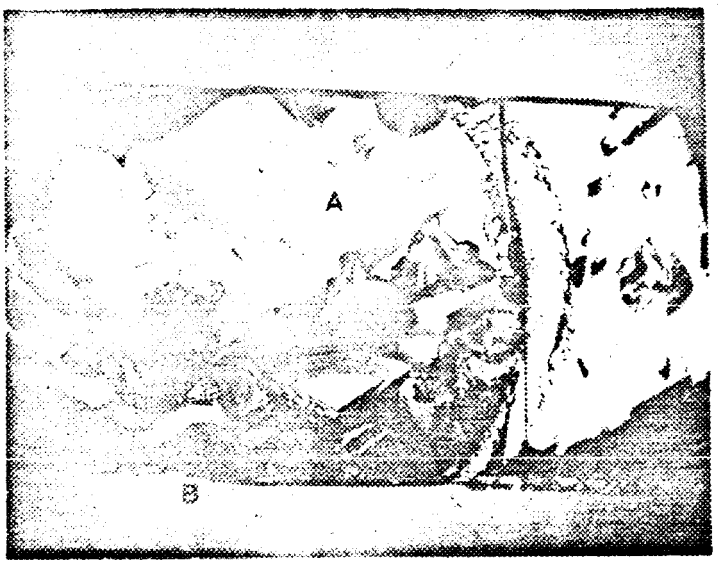

(a)

{111}B

2mm

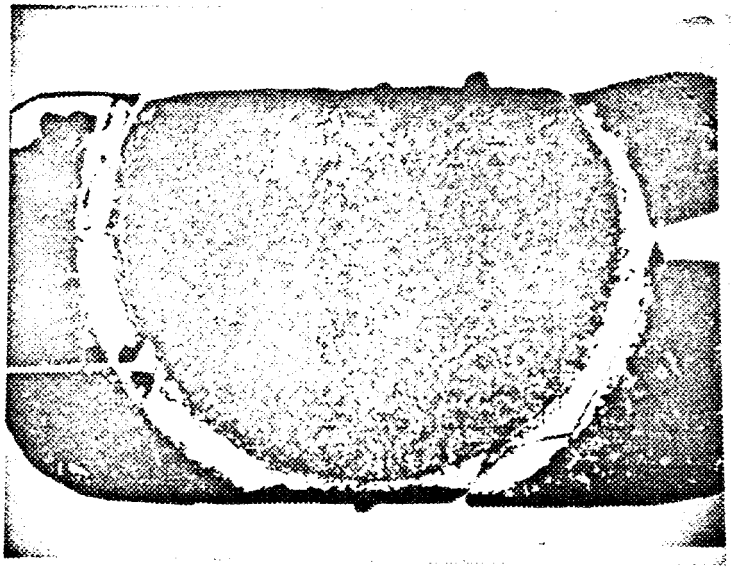

(b)

{111}B

Figure 16. Photomicrographs of stacking faults on {111}B seed surface. (a) Low stacking fault density at R_g = 2.36×10^{-6} gr cm^{-2} sec^{-1}. (b) High stacking fault density at $R_g = 10.98 \times 10^{-6}$ gr $cm^{-2} sec^{-1}$.

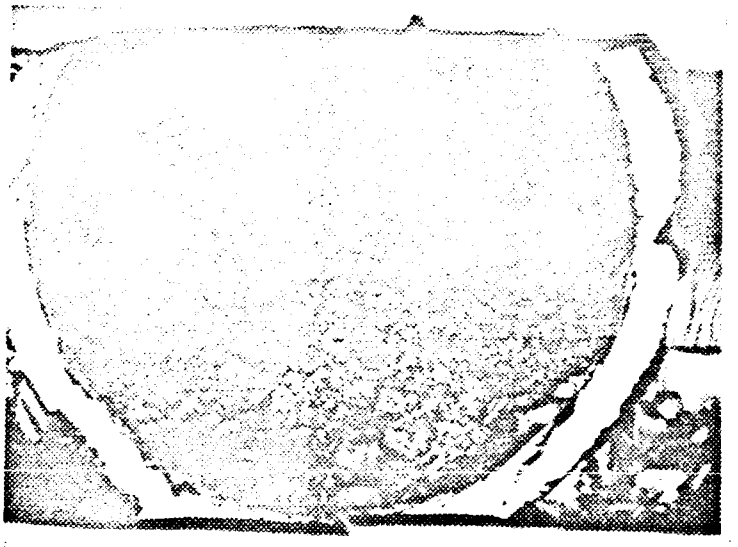

(a)

Seed {111}B with Source {100}

2mm

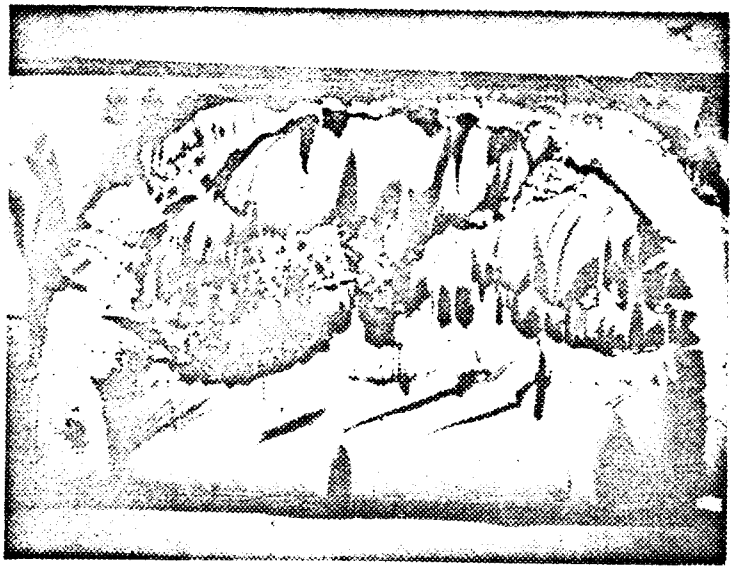

(b)

Seed {100} with Source {111}B

Figure 17. Photomicrographs of stacking fault observations. (a) {111}B seed and {100} source R_g = 10.2 x 10^{-6}gr cm^{-2} sec^{-1}. (b) {100} seed and {111}B source R_g = 3.7 x 10^{-6}gr cm^{-2} sec^{-1}.

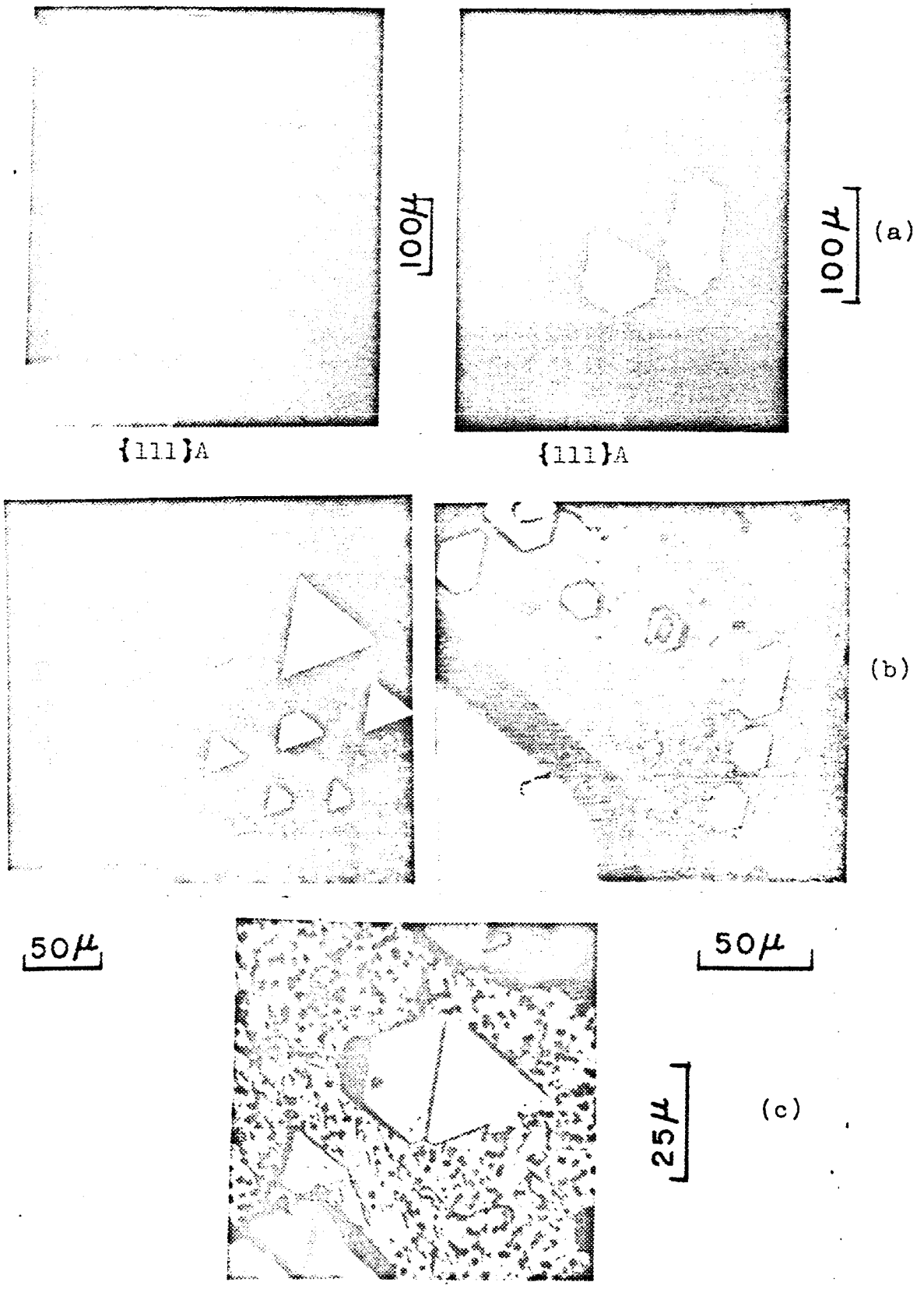

Figure 18. Photomicrographs of the "island" structure on
(a) {111}A seed
(b) {111}B seed
(c) Twinned "islands" on {111}B seed

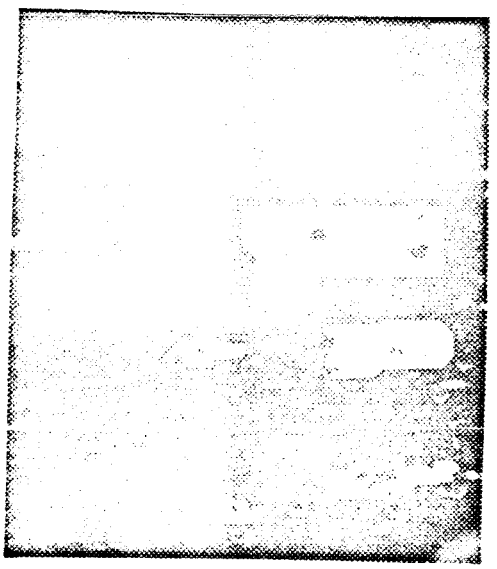

(a)

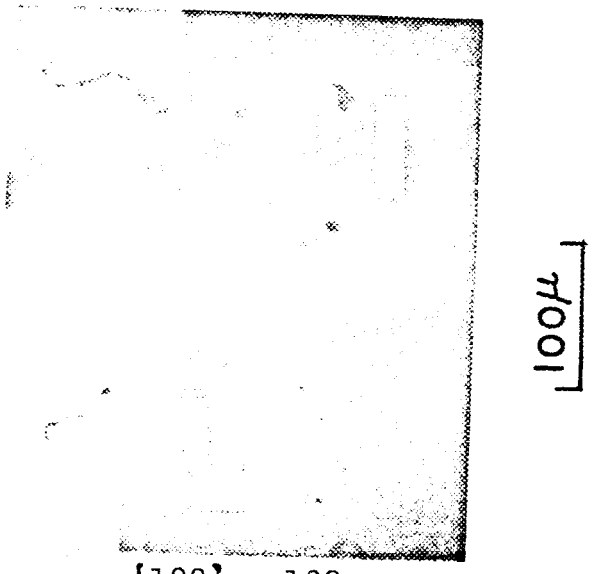

(b)

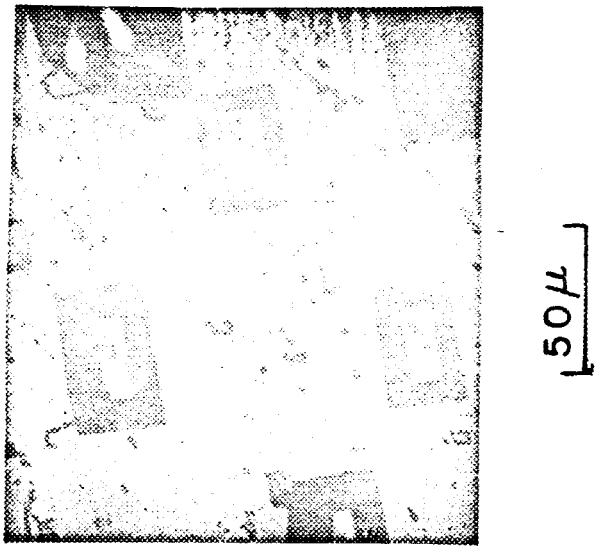

(c)

Figure 19. Photomicrographs of the "island" structure on {100} seed. (a) Truncated corner of the rectangular base. (b) and (c) Rectangular based and truncated roof-top.

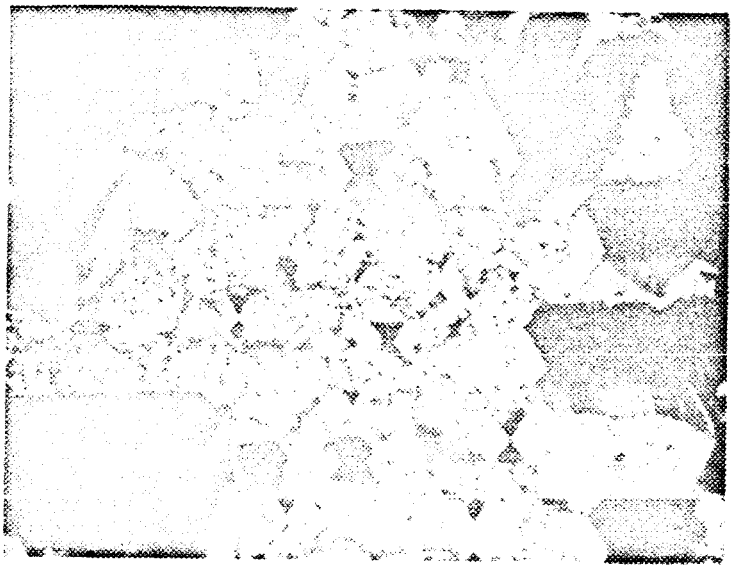

50μ

Figure 20. Photomicrographs of the "island" structure on {110} seed. Rectangular based (often) with truncated corners) "roof-top".

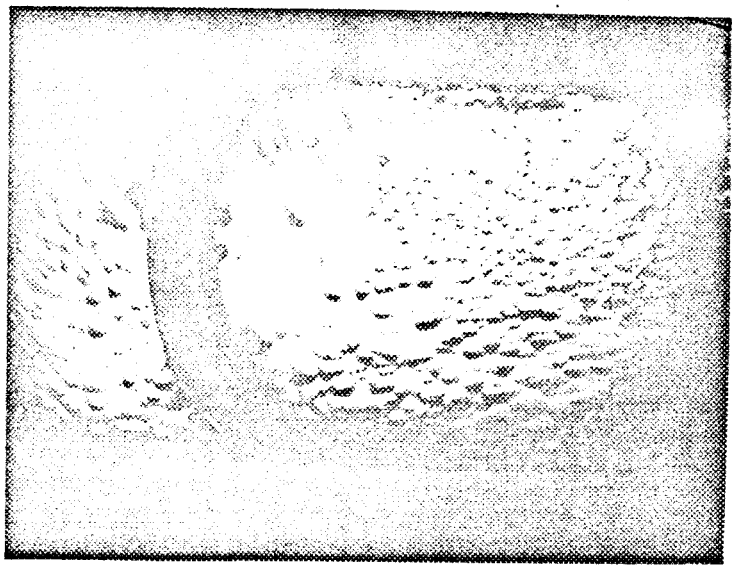

EG-67 {111}B NH_4I.

2 mm

Figure 21. Photomicrograph of the epitaxial overgrowth on {111}B seed using NH_4I.

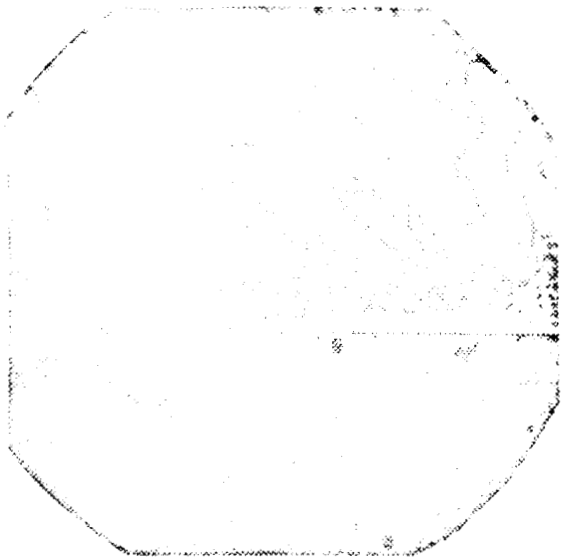

{111}B 50μ

(a)

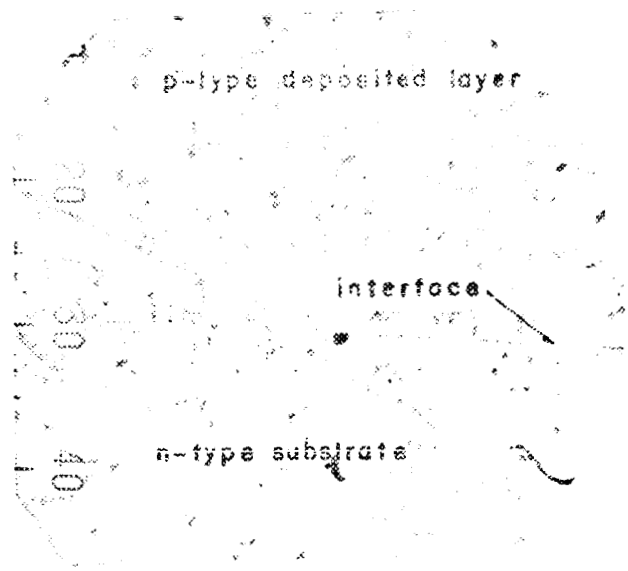

{100} 25μ

(b)

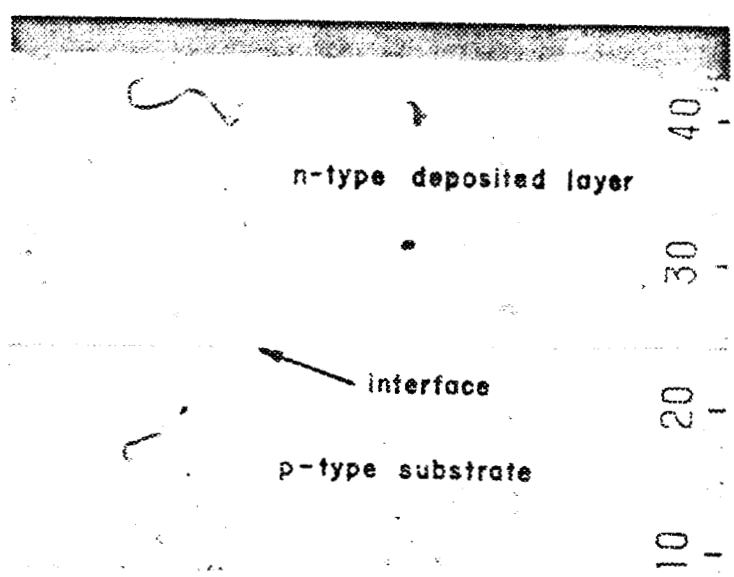

{100} d = 95μ 50μ

(c)

Figure 22. Photomicrographs of the cleaved {110} surfaces of
(a) Zn doped p-type grown layer on the n-type {111}B surface with NH_4I. Note Zn diffusion of 5.2μ beyond interface.
(b) Zn doped p-type grown layer on the n-type {100} with NH_4Cl. 2μ Zn diffusion beyond interface.
(c) Te doped n-type grown layer on the Zn doped p-type {100} with NH_4Cl.